CONF-951219--1

UCRL-JC-124307
PREPRINT

Network Asymptotics for High Contrast Impedance Tomography

Liliana Borcea
Stanford University, Stanford, California 94305

James G. Berryman
Lawrence Livermore National Laboratory, Livermore, California 94550

George C. Papanicolaou
Stanford University, Stanford, California 94305

This manuscript was prepared for the
Proceedings of the Symposium on Inverse Problems: Geophysical Applications, SIAM
Fish Camp, California
December 16-19, 1995

May 1996

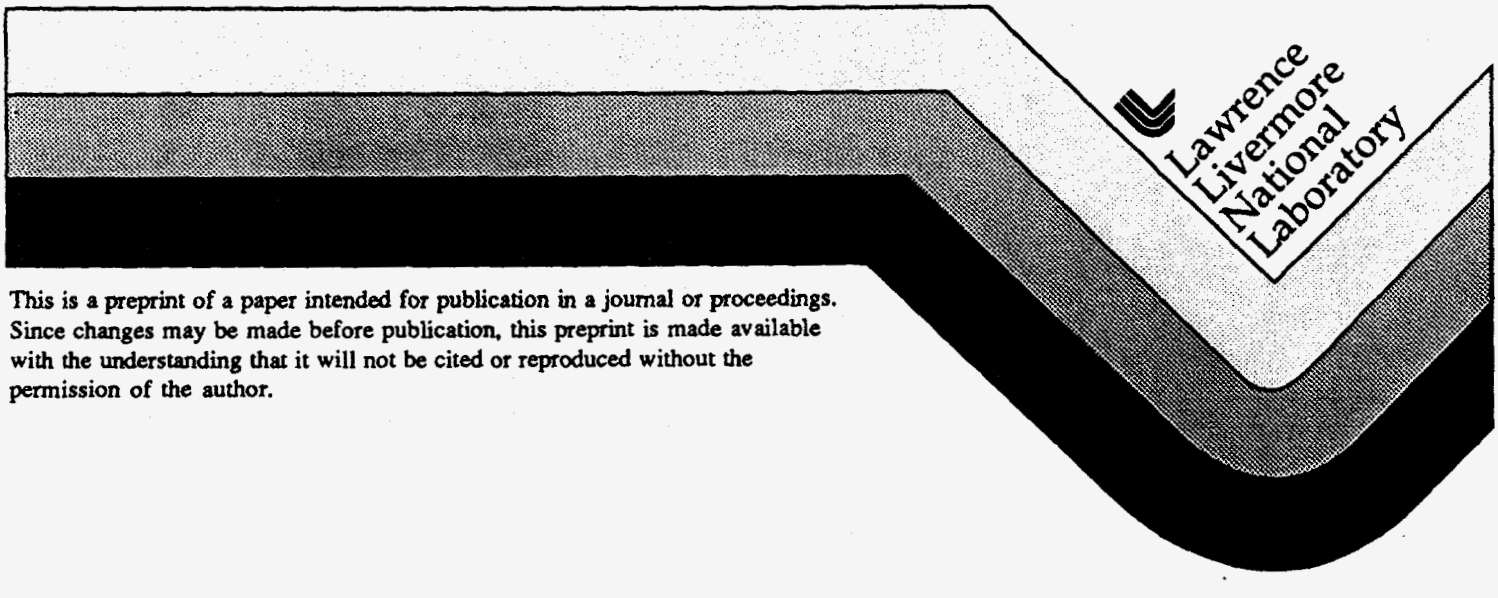

DISCLAIMER

Network Asymptotics for High Contrast Impedance Tomography

Liliana Borcea*, James G. Berryman†, and George C. Papanicolaou‡

Abstract

Fluid contaminant plumes underground are often electrically conducting and, therefore, can be imaged using electrical impedance tomography. We introduce an output least-squares method for impedance tomography problems that have regions of high conductivity surrounded by regions of lower conductivity. The high conductivity is modeled on network approximation results from an asymptotic analysis and its recovery is based on this model. The smoothly varying part of the conductivity is recovered by a linearization process as is usual. We present the results of several numerical experiments that illustrate the performance of the method.

1 Introduction

For purposes of hazard remediation, it is important to know the location and extent underground of fluid contaminant plumes. These plumes are often composed of electrically conducting fluids and, therefore, the extent of these fluids can be imaged using electrical resistance tomography (ERT) [6, 16] or electrical impedance tomography as it is more commonly known in the applied mathematics community.

Let Ω be a bounded two-dimensional region with conductivity $\sigma(x,y)$ and resistance (or impedance) $\rho(x,y) = \frac{1}{\sigma(x,y)}$. The recovery of σ from measurements of the potential ϕ at the boundary $\partial\Omega$ is the impedance tomography problem. The potential ϕ is the solution of the boundary value problem

$$\nabla \cdot (\sigma \nabla \phi) = 0 \quad \text{in} \quad \Omega \tag{1.1}$$

$$\sigma \frac{\partial \phi}{\partial n} = I \quad \text{on} \quad \partial\Omega,$$

*Scientific Computing and Computational Mathematics, Stanford University, Stanford, CA 94305, email: borcea@sccm.stanford.edu

†Lawrence Livermore National Laboratories, Environmental Programs, P. O. Box 808 L-202, Livermore, CA 94551-9900, email: berryman@s123.es.llnl.gov

‡Dept of Mathematics, Stanford University, Stanford, CA 94305, email: papanico@math.stanford.edu

where the imposed surface current density I satisfies $\int_{\partial\Omega} I dS = 0$ and the potential ϕ is unique up to a constant. An extensive review of the uniqueness and stability of the impedance tomography problem is given in [8].

We consider the recovery of the conductivity from boundary measurements when there are regions of high contrast so that linearization methods (the Born approximation) do not work. The analysis of current flow in regions with high conductivity, the direct problem, has been carried out in [10, 4]. This analysis motivates our approach to the high contrast inverse problem: we model the unknown conductivity in a special way, suggested by the analysis of the direct problem, and then estimate the parameters of the model conductivity by an output least-squares process.

In the next section we give a brief review of the analysis of high contrast conductivity problems. In section 3 we describe the inversion algorithm that we use for estimating high contrast conductivities and in section 4 we present results from numerical computations based on this algorithm. In section 5 we provide a short summary and conclusions.

2 The High Contrast Model

2.1 Description of the Model

High contrast conductivity may arise, for example, as a uniform background conductivity with highly conducting or insulating inclusions. Since in most potential applications we do not know the shape of the inclusions, it is convenient to assume that the high contrast of the conductivity (σ) arises in a general way from a continuum model of the form

$$\sigma(x) = \sigma_0 e^{-S(x)/\epsilon}. \tag{2.2}$$

Here σ_0 is a constant reference conductivity, $S(x)$ is a smooth function and ϵ is a small parameter. Variations of the function $S(x)$, the scaled logarithm of the conductivity, are amplified by the parameter ϵ, producing the high contrast of the conductivity. Media with discontinuous conductivities, like ones with inclusions of finite size, can then be viewed as particular cases of the generic model (2.2).

2.2 Review of the Asymptotic Theory

Some of the results obtained in [10, 4] for transport in media with high contrast conductivity given by (2.2) are reviewed here. Even though the analysis is done in the context of homogenization [3, 9], the conclusions are equally valid for more general circumstances.

Consider the flow problem

$$\nabla \cdot (\sigma \nabla \phi) = 0 \tag{2.3}$$

in a periodic unit cell Ω, where ϕ is the electric potential and $\sigma(x)$ is the conductivity. The flow is driven by the condition

$$< \nabla\phi >= e, \tag{2.4}$$

where $< \cdot >$ stands for the normalized average over Ω and e is a unit vector. The mean potential gradient can be specified, for example, by prescribing two different constant potentials at opposite sides of the domain.

By using Ohm's law $j = \sigma\nabla\phi$, where j is the electric current, we can also consider the dual problem

$$\begin{aligned} \nabla \times (\rho j) &= 0 \\ \nabla \cdot j &= 0 \\ < j > &= e, \end{aligned} \tag{2.5}$$

where $\rho(x) = \sigma(x)^{-1}$ is the resistance.

It is shown in references [10, 4] that, when the conductivity has logarithmically high contrast in the form (2.2), there is strong channeling of the flow at the saddle points of σ. Moreover, by using the variational formulation of the effective conductivity and resistance [4]

$$\begin{aligned} \overline{\sigma} &= \min_{<\nabla\phi>=e} < \sigma\nabla\phi \cdot \nabla\phi > \\ \overline{\rho} &= \frac{1}{\overline{\sigma}} = \min_{<j>=e,\ \nabla\cdot j=0} < \rho j \cdot j >, \end{aligned} \tag{2.6}$$

it is shown that, in the asymptotic limit of high contrast, the leading order term in the effective parameters $\overline{\sigma}$ and $\overline{\rho}$ is obtained by considering the flow only in the neighborhoods of the saddle points of σ.

To explain this flow behavior in the vicinity of the saddles, let us assume that the conductivity has a single saddle point $x_S \in \Omega$, which is oriented in the driving direction, say $e = e_1 = (1, 0)$. In a small neighborhood of x_S, the conductivity has the form

$$\sigma(x) \approx \sigma(x_S) exp[\frac{k(x - x_S)^2}{2\epsilon} - \frac{p(y - y_S)^2}{2\epsilon}], \tag{2.7}$$

where k and p are the curvatures of $S(\cdot)$ at the saddle point. In general, the saddle point can be oriented in any direction but equation (2.7) still holds if, at x_S, we introduce a local system of coordinates (x, y) such that the x direction coincides with the direction of the saddle. We take as the small region around x_S the square $| x - x_S | \leq \delta, | y - y_S | \leq \delta$ where the parameter $\delta \to 0$ in such a way that $\frac{\delta}{\epsilon} \to \infty$ as $\epsilon \to 0$.

From (2.3), the local problem near the saddle point is

$$\begin{aligned} \nabla \cdot \{\sigma(x_S) exp[\frac{k(x - x_S)^2}{2\epsilon} - \frac{p(y - y_S)^2}{2\epsilon}]\nabla\phi\} &= 0 \\ < \nabla\phi >= e_1, & \end{aligned} \tag{2.8}$$

which we solve by separation of variables. The potential $\phi(x)$ is

$$\phi(x,y) \approx \frac{1}{2} erf(\sqrt{\frac{k}{2\epsilon}}(x - x_S)), \tag{2.9}$$

correct up to an additive constant that is set to zero here. The analytical basis for (2.9) is matched asymptotic expansions. The local analysis gives the leading term (2.9) of the inner expansion valid near the saddle point. The outer expansion deals with the diffuse flow in the rest of the domain. The potential $\phi(x)$ therefore has the character of an inner layer in the direction of the saddle, the x direction in this case.

From (2.9) we compute the potential gradient

$$\nabla\phi(x,y) \approx \frac{1}{\sqrt{\frac{2\pi\epsilon}{k}}} e^{-\frac{k(x-x_S)^2}{2\epsilon}} e_1 \tag{2.10}$$

and the current

$$j = -\sigma\nabla\phi \approx -\frac{\sigma(x_S)}{\sqrt{\frac{2\pi\epsilon}{k}}} e^{-\frac{p(y-y_S)^2}{2\epsilon}} e_1. \tag{2.11}$$

We see from these expressions that when the contrast of σ is high (ϵ is small) both the current and the potential gradient are narrow Gaussians centered at x_S, which means that there is strong flow channeling around the saddle point of the conductivity. The results (2.10) and (2.11) imply that the overall, or effective, conductivity and resistance (2.6) are (see [10, 4])

$$\overline{\sigma} \approx \sigma(x_S)\sqrt{\frac{k}{p}} \quad \text{and} \quad \overline{\rho} \approx \frac{1}{\sigma(x_S)}\sqrt{\frac{p}{k}}. \tag{2.12}$$

Thus, the flow through a medium with high contrast conductivity can be approximated by the flow through a resistor having resistance $\overline{\rho}$, given by (2.12).

In more general situations, where there are more saddle points of σ in the region that are oriented in different directions, the flow still concentrates at the saddles but it follows a more complicated pattern, as in a network of channels. In the vicinity of each saddle point of the conductivity, the flow is approximated by the current through resistors given by (2.12). These resistors are connected in a network that is identified as follows: the nodes of the network are the maxima of $\sigma(x)$ and the branches are paths connecting two adjacent maxima over a saddle point. A detailed analysis is given in [4].

3 Inversion Algorithm

The asymptotic network theory described in §2 suggests that if we have flow channeling in the medium that we are trying to image, there is significant

information in the data about the resistor network that describes the flow in the high contrast regions of the conductivity. Thus, in the first step of the inversion algorithm, we should attempt to identify the relevant resistor network (channels of flow). The flow through this network is also the leading order term of the flow in the high contrast regions of σ. We could then use the conductivity estimate from the first stage of the inversion algorithm as a starting point for a second stage, trying to recover details not captured by the network. Linearizing about the conductivity of the resistor network works well at this stage because the main part of the flow through the high contrast regions of σ is already estimated, and small changes of the conductivity about it produce only small changes in the potential gradients.

3.1 Identification of the Asymptotic Resistor Network

In order to identify the resistor network that describes the flow through the high contrast regions, we *model* the unknown conductivity σ by

$$\sigma(x) \longrightarrow \sigma_b + \sum_{j=1}^{m} \chi_j(x, s_j) f_j(x, s_j). \tag{3.1}$$

Here σ_b is a uniform background in which we imbed the high contrast modules $f_j(\cdot)$. Each high contrast module is of the form $f_j(\cdot) \sim e^{\frac{S_j(x)}{\epsilon}}$, with support in the interior of Ω, and consists of a saddle point surrounded by two maxima and two minima. The vectors of parameters s_j describe the structure of the modules $f_j(\cdot)$ by specifying the position of the saddle points, their orientation, the curvatures at the saddle, the contrast, etc. The modules $f_j(\cdot)$ are localized with the smooth cutoff functions $\chi_j(\cdot)$. Detailed descriptions are given in section 4.2.

Since conductivities defined by (3.1) are completely determined by the parameters s_j, $j = 1, \ldots m$, we estimate them by minimizing the error between the solution with these parameters and the observed data. Thus, we estimate the s_j, $j = 1, \ldots m$ by minimizing the mean-square error

$$E(s_1, \ldots s_m) = \sum_{i=1}^{M} \sum_{k=1}^{N} \left[\psi_k^{(i)} - \phi_k^{(i)}(s_1, \ldots s_m) \right]^2, \tag{3.2}$$

where the index of summation k runs through the data points on the boundary and i labels the pair of electrodes at which the current is injected into the domain. The potential measured on the boundary is $\psi_k^{(i)}$, while $\phi_k^{(i)}(\cdot)$ is the potential on the boundary calculated by solving the partial differential equation (1.1) with the current best estimate of a conductivity of the form (3.1). This is an output least-squares estimation method, parametrized with high contrast conductivities of the form (3.1).

Introducing a model of the form (3.1) for the conductivity is a form of *regularization* [17] for the output least squares problem (3.2). It is

particularly well suited to high contrast problems, as we know from the analysis of the direct problem summarized in section 2.2.

To describe our minimization algorithm, we assume at first for simplicity that we have only one high contrast module ($m = 1$) in (3.1). When the vector of parameters $s \in \mathbb{R}^p$ changes by Δs, the mean-square error (3.2) changes by

$$E(s) + \Delta E \approx \sum_{i=1}^{M} \sum_{k=1}^{N} \left[\psi_k^{(i)} - \phi_k^{(i)}(s) - \sum_{j=1}^{p} \frac{\partial \phi_k^{(i)}}{\partial s_j} \Delta s_j \right]^2, \tag{3.3}$$

where we use the fact that, when the change in s is small, we have

$$\phi_k^{(i)}(s + \Delta s) \approx \phi_k^{(i)}(s) + \sum_{j=1}^{p} \frac{\partial \phi_k^{(i)}}{\partial s_j} \Delta s_j. \tag{3.4}$$

From (3.3) the change in the error is

$$\Delta E \approx \sum_{j=1}^{p} \sum_{l=1}^{p} A_{jl} \Delta s_j \Delta s_l - 2 \sum_{j=1}^{p} b_j \Delta s_j. \tag{3.5}$$

Here we introduced the symmetric positive definite sensitivity matrix

$$A_{jl} = \sum_{i=1}^{M} \sum_{k=1}^{N} \frac{\partial \phi_k^{(i)}}{\partial s_j} \frac{\partial \phi_k^{(i)}}{\partial s_l} \tag{3.6}$$

and the vector

$$b_j = \sum_{i=1}^{M} \sum_{k=1}^{N} \left[\psi_k^{(i)} - \phi_k^{(i)}(s) \right] \frac{\partial \phi_k^{(i)}}{\partial s_j}, \tag{3.7}$$

whose components measure the current data misfit weighted by the sensitivity of the potential to changes in s_j. The decrease in the error ΔE is maximized when the parameters Δs satisfy [12] the linear equations

$$A \Delta s = b \tag{3.8}$$

and then the change in the mean-square error is

$$\Delta E \approx -\Delta s^T A \Delta s \leq 0. \tag{3.9}$$

This Gauss-Newton algorithm [7], given by (3.6) - (3.8), does not work well here because the matrix A, as defined by (3.6), is ill-conditioned. Some of the components of the parameter vector s change faster than others. For example, when the contrast is high and the flow concentration at the saddle point is strong, the position of the saddle point is recovered after a few iterations while the contrast converges slowly. We avoid this difficulty by updating the vector of parameters s one component at a time, instead of

all at once. This approach has, in addition, the advantage of allowing us to terminate the updating of parameters that have converged before the end of the overall iteration process. The change in the j^{th} component of s that maximizes the decrease in the error is easily found to be

$$\Delta s_j = \frac{\sum_{i=1}^{M}\sum_{k=1}^{N}\left[\psi_k^{(i)} - \phi_k^{(i)}(s)\right]\frac{\partial \phi_k^{(i)}}{\partial s_j}}{\sum_{i=1}^{M}\sum_{k=1}^{N}\left(\frac{\partial \phi_k^{(i)}}{\partial s_j}\right)^2} = \frac{b_j}{A_{jj}} \tag{3.10}$$

and then

$$\Delta E \approx -(\Delta s_j)^2 \sum_{i=1}^{M}\sum_{k=1}^{N}\left(\frac{\partial \phi_k^{(i)}}{\partial s_j}\right)^2 = -A_{jj}(\Delta s_j)^2 \leq 0. \tag{3.11}$$

The change in the parameters s depends both on the error at the boundary and on the sensitivity coefficients $\frac{\partial \phi_k^{(i)}}{\partial s_j}$. Thus, at each step of the iteration, we must solve the elliptic problems

$$\begin{aligned} \nabla \cdot (\sigma \nabla \phi) &= 0 \\ \sigma \frac{\partial \phi}{\partial n} &= f \text{ on } \partial\Omega \\ \phi(0, s) &= 0 \end{aligned} \tag{3.12}$$

and

$$\begin{aligned} \nabla \cdot \left(\sigma \nabla \frac{\partial \phi}{\partial s_i}\right) &= -\nabla \cdot \left(\frac{\partial \sigma}{\partial s_i} \nabla \phi\right) \\ \sigma \frac{\partial}{\partial n}\left(\frac{\partial \phi}{\partial s_i}\right) &= 0 \text{ on } \partial\Omega \\ \frac{\partial \phi}{\partial s_i}(0, s) &= 0 \text{ for } i = 1, \ldots p. \end{aligned} \tag{3.13}$$

However, since small changes in the components of s lead to an updated potential of the form (3.4), we need to solve (3.12) only once every p iterations.

In the Gauss-Newton method we approximate the Hessian of the mean square error (3.1) by the first derivatives of the estimated potential (3.4). Second derivatives are difficult to calculate and therefore omitted. The success of the method depends on the negligibility of second derivatives [7] and to insure that they are negligible, we scale the update in the parameters (3.10) by a factor $\lambda_c > 0$. The algorithm, then called a damped Gauss-Newton method [7], is globally convergent for many nonlinear least-squares problems, including large residual problems [7]. In our computations we choose the scaling parameter λ_c so that the change in s_j is smaller than 15%.

3.2 Identification of Features of the Conductivity that are Neglected by the Asymptotic Theory

The resistor network identified by the algorithm described in §3.1 is in general only a rough estimate of the conductivity $\sigma(x)$. In order to improve its resolution we must also identify low contrast features of $\sigma(x)$ that are not captured by the asymptotic resistor network theory. This is done by linearizing about the network conductivity estimated by the algorithm described in the previous section. In this section we define the linearized problem and explain why it works at this stage of the inversion algorithm.

For a reference medium with conductivity $\sigma_r(x)$ of form (3.1), we have

$$\nabla \cdot [\sigma_r(x)\nabla\phi_r(x)] = 0 \quad \text{in} \quad \Omega$$

(3.14)

$$\sigma_r \frac{\partial \phi_r}{\partial n} = I \quad \text{on} \quad \partial\Omega,$$

where $\phi_r(x)$ is the reference potential. Suppose that

(3.15) $$\sigma(x) = \sigma_r(x) + \delta\sigma(x), \quad \text{where}$$

Then problem (1.1) can then be written as

$$\nabla \cdot [\sigma_r(x)\nabla\psi(x)] = -\nabla \cdot [\delta\sigma(x)\nabla\phi(x)] \quad \text{in} \quad \Omega$$

(3.16)

(3.17) $$(\sigma + \delta\sigma)\frac{\partial \phi}{\partial n} = I \quad \text{on}$$

where $\psi(x) = \phi(x) - \phi_r(x)$. The perturbed potential gradient $\nabla\psi(x)$ that is due to the change $\delta\sigma(x)$ of the reference conductivity is assumed to be much smaller than the reference potential gradient $\nabla\phi_r(x)$, so we linearize equation (3.16) to obtain

(3.18) $$\nabla \cdot [\sigma_r(x)\nabla\psi(x)] \approx -\nabla \cdot [\delta\sigma(x)\nabla\phi_r(x)] \quad \text{in} \quad \Omega.$$

Equation (3.18) is linear in $\delta\sigma(x)$. Linearization is justified in the second stage of our inversion algorithm because, as we explained in §2.2, the resistor network given by $\sigma_r(x)$ determines the main part of the flow in the high contrast regions of the medium. Small changes of the reference conductivity can only produce small changes in the potential gradient, so linearization (3.18) can be used.

Inversion of the linearized problem (3.18) recovering $\delta\sigma(x)$ has been the topic of numerous studies and an extensive literature on recovery algorithms is available (for example, [1, 6, 16]). In our computations we used an adjoint representation [15] that requires less computation than the usual algorithms that are based on Green's functions.

4 Numerical Results

All numerical computations were done using the PLTMG [2] software package. This is an adaptive multigrid solver for elliptic PDEs in two dimensions that we tested carefully in [5].

4.1 One Channel Model

In this section we present numerical results obtained with the inversion algorithm described in §3 for conductivities that have only one saddle point in the domain. An example of such a conductivity is

$$\sigma(x) = \sigma_b + \chi(x,s)f(x,s), \tag{4.1}$$

where σ_b is a uniform background $f(\cdot)$ is a high contrast module that has a saddle point surrounded by two maxima and two minima and $\chi(\cdot)$ is a cutoff function that localizes $f(\cdot)$. We model the high contrast module by

$$\begin{aligned} f(x,s) = \sigma_0 \exp\{\frac{1}{\epsilon}\sin[\alpha((x-x_s)\cos\theta + (y-y_s)\sin\theta)] \times \\ \sin[\beta((y-y_s)\cos\theta - (x-x_s)\sin\theta)]\}, \end{aligned} \tag{4.2}$$

where (x_s, y_s) is the location of the saddle point of the conductivity, θ is the orientation of the saddle and ϵ determines the contrast. The function $f(\cdot)$ in (4.2) is periodic with periods determined by α and β, which also determine the curvatures at the saddle. The constant σ_0 controls the height of the saddle. Thus, the high contrast conductivity module is completely described by the eight-component vector

$$s = (\sigma_b, \sigma_0, \alpha, \beta, x_s, y_s, \theta, \epsilon). \tag{4.3}$$

The high contrast module $f(\cdot)$ is tapered with the C^1 cutoff function

$$\begin{aligned} \chi(x,s) = g((x-x_s)\cos\theta + (y-y_s), \alpha) \times \\ g(-(x-x_s)\sin\theta + (y-y_s)\cos\theta), \beta), \end{aligned} \tag{4.4}$$

where

$$g(\xi,\gamma) = \begin{cases} \sin^3[\frac{\pi}{2}(\xi+\frac{\pi}{\gamma})/d] & \text{for } -\frac{\pi}{\gamma} \le \xi \le -\frac{\pi}{\gamma}+d \\ -\sin^3[\frac{\pi}{2}(\xi-\frac{\pi}{\gamma})/d] & \frac{\pi}{\gamma}-d \le \xi \le \frac{\pi}{\gamma} \\ 1 & -\frac{\pi}{\gamma}+d \le \frac{\pi}{\gamma}-d \\ 0 & |\xi| \ge \frac{\pi}{\gamma}. \end{cases} \tag{4.5}$$

The parameter d in (4.5) controls the sharpness of the cutoff and it is kept constant throughout the numerical experiments.

The data that we use in the numerical experiments are generated numerically with a synthetic model of the form (4.1) and PLTMG. An

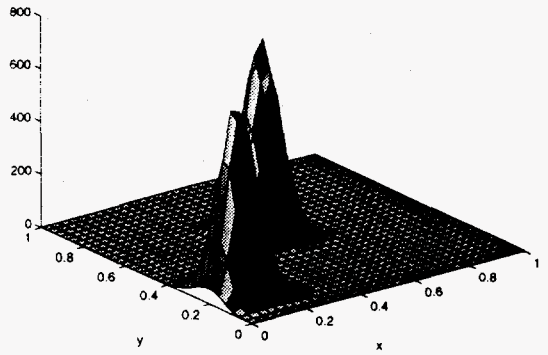

FIG. 1. *Model conductivity (Contrast = 369)*

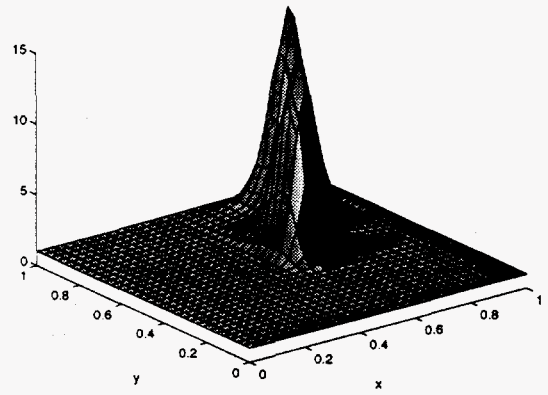

FIG. 2. *Initial conductivity guess (Contrast = 14.7)*

example of a conductivity used to generate data is shown in Fig. 1. In a uniform background, $\sigma_b = 2$, we have embedded a high contrast module $(\max(\sigma)/\min(\sigma) = 369)$ that has a saddle at $(x_s, y_s) = (0.3, 0.4)$ which is oriented at an angle $\pi/4$ from the axes.

As a starting point in the iterative process of reconstructing the model σ shown in Fig. 1, we consider the conductivity shown in Fig. 2. Even though the initial guess is of the same form (4.1) as the model, the set of parameters $\{s\}$ describing it is very different. The background conductivity is $\sigma_b^{init} = 1$; the saddle is situated at $(x_s, y_s)^{init} = (0.7, 0.7)$; and the contrast is 14.7. The initial relative error in the conductivity (see Fig. 3) is very high around the initial guess of the position of the saddle ($\sim 600\%$) and about 60% elsewhere in the domain.

In the reconstruction process, the data consists of the value of the potential at points placed a distance $h = 1/32$ apart along the sides ($x = 0$

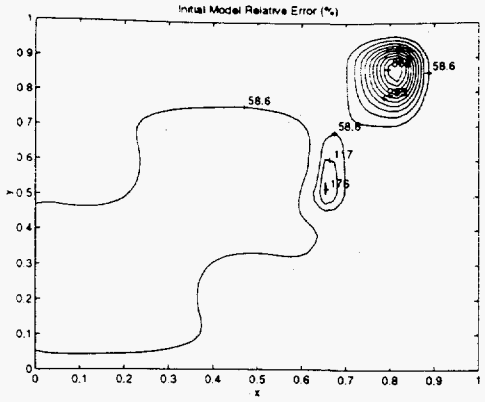

FIG. 3. *L_∞ initial relative error in the conductivity*

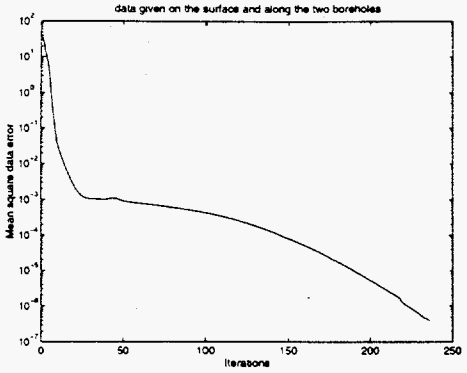

FIG. 4. *Evolution of the mean square data error*

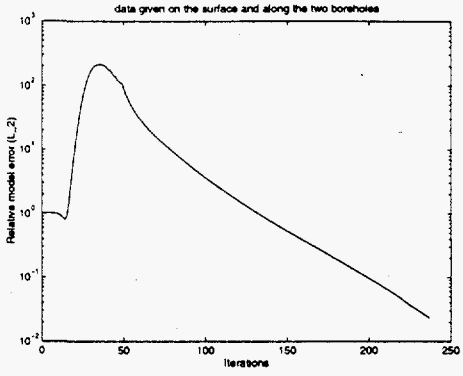

FIG. 5. *Evolution of the L_2 relative error in the conductivity*

and $x = 1$) and the surface boundary ($y = 1$). Current is injected with two different pairs of electrodes located at (0,0.5), (1,0.5) and (0,0.3), (0.5,1), respectively.

The evolution of the mean-square data error during the iteration process is shown in Fig. 4. The algorithm reduces this error monotonically. However, it does not guarantee reduction of the error in the conductivity and as shown in Fig. 5. At some stage of the iteration process the error in the model actually increases. This behavior is due to the strong nonlinearity of the problem and is more subdued in experiments with contrast of order ten. After 250 iterations, the relative error in the conductivity in the L_2 norm is reduced by two orders of magnitude. The final relative error in the model in the L_∞ norm (see Fig. 6) is only a few percent so the model conductivity is recovered quite well.

Some of the components of the vector of parameters s describing the model conductivity are recovered more quickly than others during

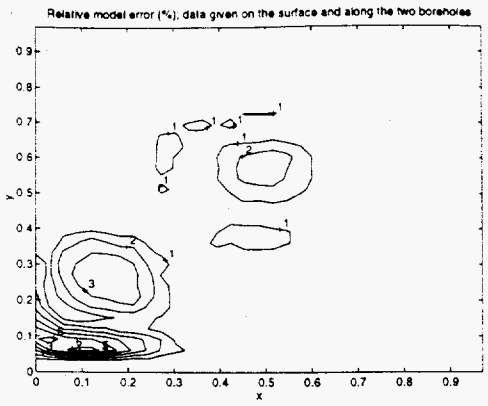

FIG. 6. *Relative model error (%)*

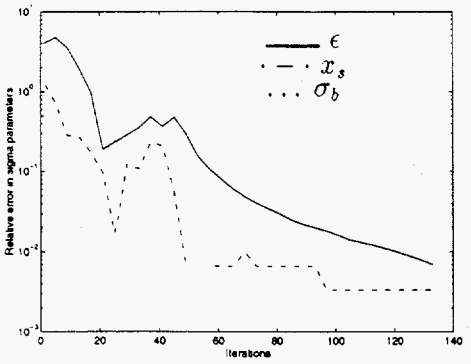

FIG. 7. *Convergence of high contrast module parameters. Contrast of* $\sigma = 10^4$

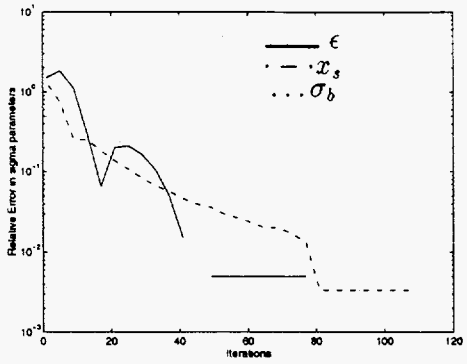

FIG. 8. *Convergence of high contrast module parameters. Contrast of* $\sigma = 14$

reconstruction. For example, the position of the saddle point is expected to be easily recovered in experiments with high contrast. For low contrasts, flow channeling is weak so the position of the saddle is harder to recover. In Figs. 7 and 8, we show the evolution of the relative error in three parameters (ϵ, σ_b, and x_s) obtained from two numerical experiments that assume contrasts 10^4 and 14, respectively. When the contrast is high, the position of the saddle and the uniform background are recovered more quickly than the parameter ϵ that controls the contrast; when the contrast is lowered to 14, the position of the saddle is instead the *last* parameter to be recovered. The numerical experiment for reconstructing the model conductivity shown in Fig. 1 was repeated with data to which 5% noise has been added. The noise is simulated with independent, identically distributed Gaussian random variables. The starting point in the iteration is as before (see Fig. 2). From Fig. 9 we see that the mean-square error decreases to about 10^{-2} in 50 iterations and

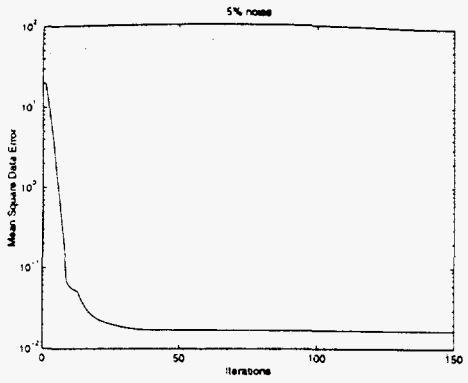

FIG. 9. *Evolution of mean square data error (5% noise)*

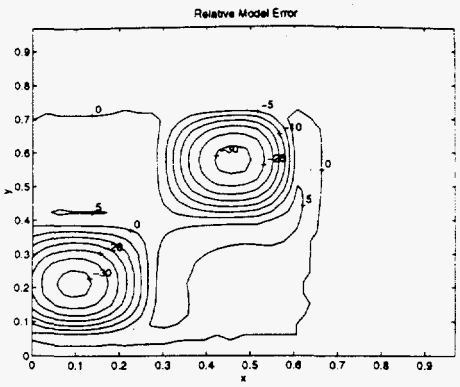

FIG. 10. L_∞ *conductivity error (5% noise)*

remains unchanged after that. The relative error in the model in the L_∞ norm, shown in Fig. 10, shows that, even with very noisy data, the algorithm recovers the background conductivity, the position and orientation of the channel and the support of the high contrast region. The error is high ($\sim 30\%$) only around the maxima of the conductivity where the potential gradient is nearly zero and so the inverse problem is ill-posed in this region. The quality of the results improves when the noise level is reduced. For example, with 1% noise the relative model error is smaller than 10%.

4.2 More Complex Systems

If the model conductivity consists of a high contrast module embedded in a variable background, we can perform the inversion in two steps. In the first step of the inversion process, we repeat the preceding analysis looking for a conductivity of the form (4.1) that fits the data best. In the second step of the inversion process, we improve the quality of the image by linearizing about the conductivity given in the first step. Results obtained show that the quality of the image improves in the background.

When there are multiple channels present, we can try to identify them all at once or one at a time. We have used the second approach in imaging the conductivity of media with two and three channels of flow. If the channels are well separated, the algorithm works well. The channels are found sequentially, one by one, starting with the one closest to the boundary and ending with the ones in the interior of the flow domain. This is similar to the method of matching pursuit [13].

More general high contrast conductivity distributions are to be anticipated in practice. To provide some examples, we have considered high contrast Gaussian conductivity perturbations. Figure 11 shows the target conductivity. We have tried to reconstruct this conductivity using a single

Gaussian, two Gaussians, and three Gaussians. For a single Gaussian module, the result is expected to be a poor fit to the target model. We pursued this example anyway to determine whether the single Gaussian would fit just one of the peaks well and ignore the other, or whether it might straddle the two peaks while fitting neither very well. The result (not shown) was that the single Gaussian module tried to straddle the two peaks and does a rather poor job reducing the least squares-error functional.

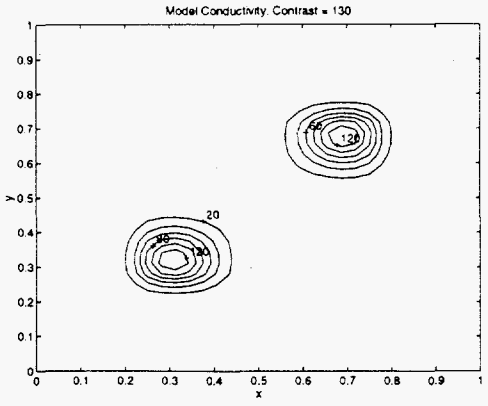

FIG. 11. *Target conductivity used in Gaussian search examples*

A reconstruction algorithm using two Gaussian modules was much more successful at fitting the target conductivity as can be observed in Figs. 12-14. The mean square data for a single Gaussian mopdule was about twice as high and could not be improved. For two Gaussians, the overall fit is reasonable after about 10 iterations and continues to improve as the algorithm searches for the optimum values for the Gaussian height and width parameters.

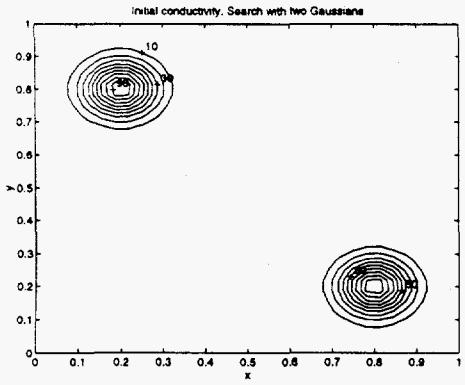

FIG. 12. *Starting conductivity σ for two Gaussian search.*

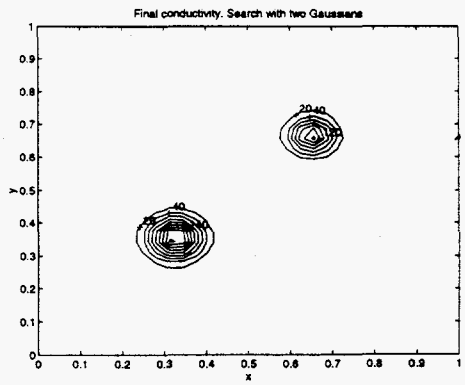

FIG. 13. *Final conductivity σ for two Gaussian search.*

Using three Gaussians in the search produced significantly better results

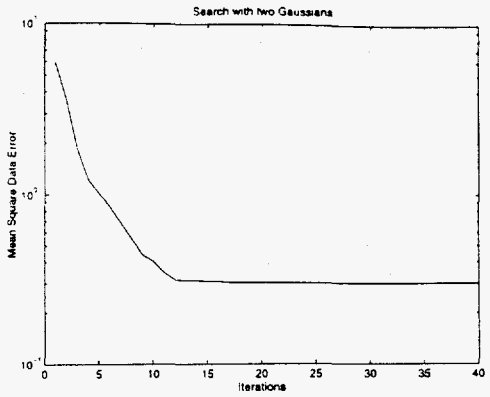

FIG. 14. *Evolution of mean square data error for two Gaussian search.*

as is observed in Figs. 15-17. Only two peaks are observed in the final reconstruction because two of the three Gaussians have coalesced. The mean square data error is an order of magnitude smaller than the case with two Gaussians, showing that there are clear advantages to using more, and therefore more flexible, modules in the reconstruction algorithm.

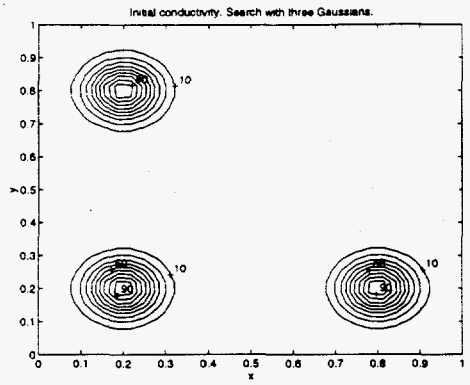

FIG. 15. *Starting conductivity σ for three Gaussian search.*

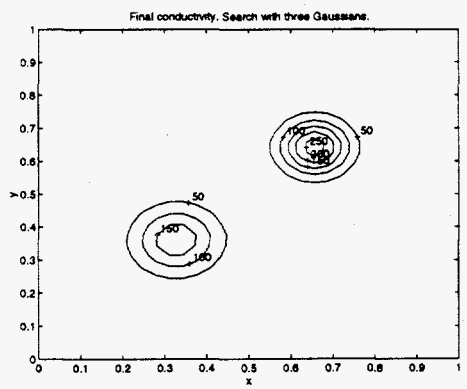

FIG. 16. *Final conductivity σ for three Gaussian search.*

5 Summary

We have introduced an inversion algorithm for tomographic imaging of media with large variations in the conductivity. The algorithm is based on the results of an asymptotic analysis of the forward problem in media with high contrast. This analysis shows that when the contrast of the conductivity is high, the flow can be approximated reasonably well by that of a resistor network. The network accounts for the main part of the flow

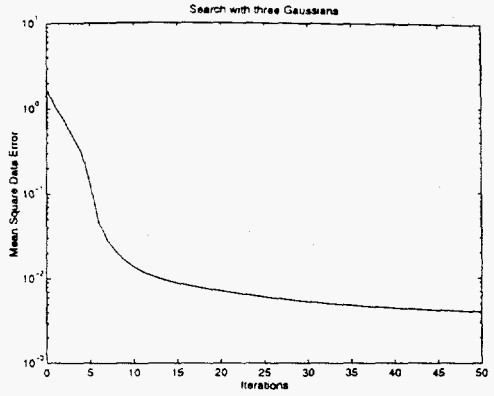

FIG. 17. *Evolution of mean square data error for three Gaussian search.*

and neglects the residual low contrast features of the conductivity. We introduce a new parametrization of the conductivity based on the resistor network theory and use an output least-squares approach for identifying the network. We have shown that this parametrization acts to regularize the inverse problem. The conductivity estimated in this first stage of the algorithm may be used as a reference conductivity in a second stage, where we identify low contrast features not captured by the network.

We have assessed the performance of the algorithm with several numerical experiments and have shown that it is stable and successful in imaging high contrast conductivities in many situations. In our first set of experiments, the inversion algorithm used high contrast modules that are somewhat rigid [see (4.1)-(4.5)], in the sense that they require the peaks of the conductivity surrounding the channel to have the same height. A second set of experiments using more flexible conductivity modules to represent the model (in the present case two or more Gaussian perturbations to a constant background conductivity) has shown that a degree of flexibility in the functionals used to parametrize the model space can produce much better fits to both the data and to the desired conductivity model without introducing undesirable instabilities.

ACKNOWLEDGMENTS

We thank F. Natterer for several useful discussions and for pointing out the use of adjoint representations for solving (3.13). The work of J. Berryman was performed under the auspices of the U. S. Department of Energy by the Lawrence Livermore National Laboratory under contract No. W-7405-ENG-48 and supported in part by the Geosciences Research Program within the Office of Basic Energy Sciences, Division of Engineering and Geosciences. It was also supported in part by AFOSR grant F49620-94-1-0436. The work of L. Borcea and G. Papanicolaou was supported by NSF grant DMS96-22854 and AFOSR grant F49620-94-1-0436.

References

[1] Allen, A. and Santosa, F., 1991, *Stability and resolution analysis of a linearized problem in electrical impedance tomography*, Inverse Problems, **7**, pp. 515-533.

[2] Bank, E.R., 1990, *PLTMG: A Software Package for Solving Elliptic Partial Differential Equations*, SIAM.

[3] Bensoussan, A., Lions, J.L., Papanicolaou, G.C., 1978, *Asymptotic Analysis for Periodic Structures*, North-Holland, Amsterdam.

[4] Borcea, L., Papanicolaou, G.C., 1996, *Network approximation for transport properties of high contrast materials*, submitted SIAM Applied Mathematics.

[5] Borcea, L., Papanicolaou, G.C., 1996, *A hybrid numerical method for high contrast conductivity problems*, submitted J. Computational and Applied Math..

[6] Daily, W.D., A. Ramirez, D. LaBrecque and Nitao, J., 1992, *Electrical resistivity tomography of vadose water movement*, Water Resources Res. **28**, pp. 1429-1442.

[7] Gill, P.E., Murray, W. and Wright, M.H., 1981, *Practical Optimization*, Academic Press, London.

[8] Isakov, V., 1993, *Uniqueness and stability in multi-dimensional inverse problems*, Inverse Problems, 9, pp. 579-621.

[9] Jikov, V.V., Kozlov, S.M., Oleinik, O.A., 1994, *Homogenization of Differential Operators and Integral Functional*, Springer-Verlag, Berlin Heidelberg.

[10] Kozlov, S.M., 1989, *Geometric aspects of averaging*, Russian Math. Surveys 44:2, pp. 91-144.

[11] *LAPACK User's Guide*, 1992, SIAM.

[12] Lu, S.-Y., and Berryman, J.G., 1990, *Inverse scattering, seismic traveltime tomography, and neural networks*, Int. J. of Imaging Systems and Techn., Vol. 2, pp. 112-118.

[13] Mallat, S. and Zhang, Z., 1993, *Matching pursuit in a time-frequency dictionary*, IEEE Trans. Signal Processing, **41**, pp. 3397-3415.

[14] Mitchell, A.R., 1969, *Computational Methods in Partial Differential Equations*, J. Wiley, New York.

[15] Natterer, F., 1986, *The Mathematics of Computerized Tomography*, John Wiley and Sons.

[16] Ramirez, A., Daily, D.W., LaBrecque, D., Owen, E. and Chesnut D., 1993, *Monitoring an underground steam injection process using electrical resistance tomography*, Water Resources Res., **29**, pp. 73-87.

[17] Tikhonov, A. and Arsénine, V., 1976, *Méthodes de Résolution de Problèmes Mal Posés*, Éditions Mir, Moscow.